# Improved Orbit Determination and Forecasts with an Assimilative Tool for Satellite Drag Specification

**Marcin D. Pilinski**
*ASTRA LLC., Boulder, CO 80301*

**Geoff Crowley**
*ASTRA LLC., Boulder, CO 80301*

**Eric Sutton**
*Air Force Research Labs, Kirtland AFB, NM 87117*

**Mihail Codrescu**
*Space Weather Prediction Center, National Oceanic and Atmospheric Administration, Boulder, CO 80305*

## 1. ABSTRACT

Much as aircraft are affected by the prevailing winds and weather conditions in which they fly, satellites are affected by the variability in density and motion of the near earth space environment. Drastic changes in the neutral density of the thermosphere, caused by geomagnetic storms or other phenomena, result in perturbations of LEO satellite motions through drag on the satellite surfaces. This can lead to difficulties in locating important satellites, temporarily losing track of satellites, and errors when predicting collisions in space. As the population of satellites in Earth orbit grows, higher space-weather prediction accuracy is required for critical missions, such as accurate catalog maintenance, collision avoidance for manned and unmanned space flight, reentry prediction, satellite lifetime prediction, defining on-board fuel requirements, and satellite attitude dynamics.

We describe ongoing work to build a comprehensive nowcast and forecast system for specifying the neutral atmospheric state related to orbital drag conditions. The system outputs include neutral density, winds, temperature, composition, and the satellite drag derived from these parameters. This modeling tool is based on several state-of-the-art coupled models of the thermosphere-ionosphere as well as several empirical models running in real-time and uses assimilative techniques to produce a thermospheric nowcast. This software will also produce 72 hour predictions of the global thermosphere-ionosphere system using the nowcast as the initial condition and using near real-time and predicted space weather data and indices as the inputs.

In this paper, we will review the driving requirements for our model, summarize the model design and assimilative architecture, and present preliminary validation results. Validation results will be presented in the context of satellite orbit errors and compared with several leading atmospheric models. As part of the analysis, we compare the drag observed by a variety of satellites which were not used as part of the assimilation-dataset and whose perigee altitudes span a range from 200 km to 700 km.

## 2. INTRODUCTION

There are numerous motivations for improving the state of the art modeling of the orbital drag environment. As the population of satellites in Earth orbit grows with time, higher orbital prediction accuracy is required for critical missions, such as accurate catalog maintenance, collision avoidance for manned and unmanned space flight, reentry prediction, satellite lifetime prediction, specifying on-board fuel requirements, and satellite attitude dynamics. Collision avoidance is complicated by many false positive alerts which are caused by large uncertainties in orbit prediction. These orbit prediction errors are in turn caused largely by inaccurate atmospheric density forecasts. These activities are critical to the operational needs of LEO-asset management and to Space Situational Awareness efforts.

The Committee for the Assessment of NASA's Orbital Debris Programs notes that the ability to maintain a catalogue of space object orbits feeds into NASA and MDA debris and breakup assessment models which support critical needs in hazard detection and risk assessment ("Limiting Future Collision Risk to Spacecraft: An Assessment of NASA's Meteoroid and Orbital Debris Programs"). This capability for catalogue maintenance, critical to DoD and NASA missions, is complicated by the fact that much of the LEO space object population has orbits which are continuously perturbed by satellite drag.

Thus, improvements in satellite-drag prediction capability are needed and motivate the development of the Dragster system to specify more accurate atmospheric densities and to enhance conjunction analysis accuracy.

Fig. 1 illustrates the Dragster approach. In the top left, resident space object observations are assimilated into Dragster (top right). Dragster's ensemble of atmospheric models is then used along with operational atmospheric-forcing data to generate a set of satellite drag forecasts akin to a hurricane track prediction (lower right). In the future, this information will feed into existing orbit propagation tools to improve satellite position nowcasts and forecasts and reduce errors in conjunction analysis versus the currently available methods.

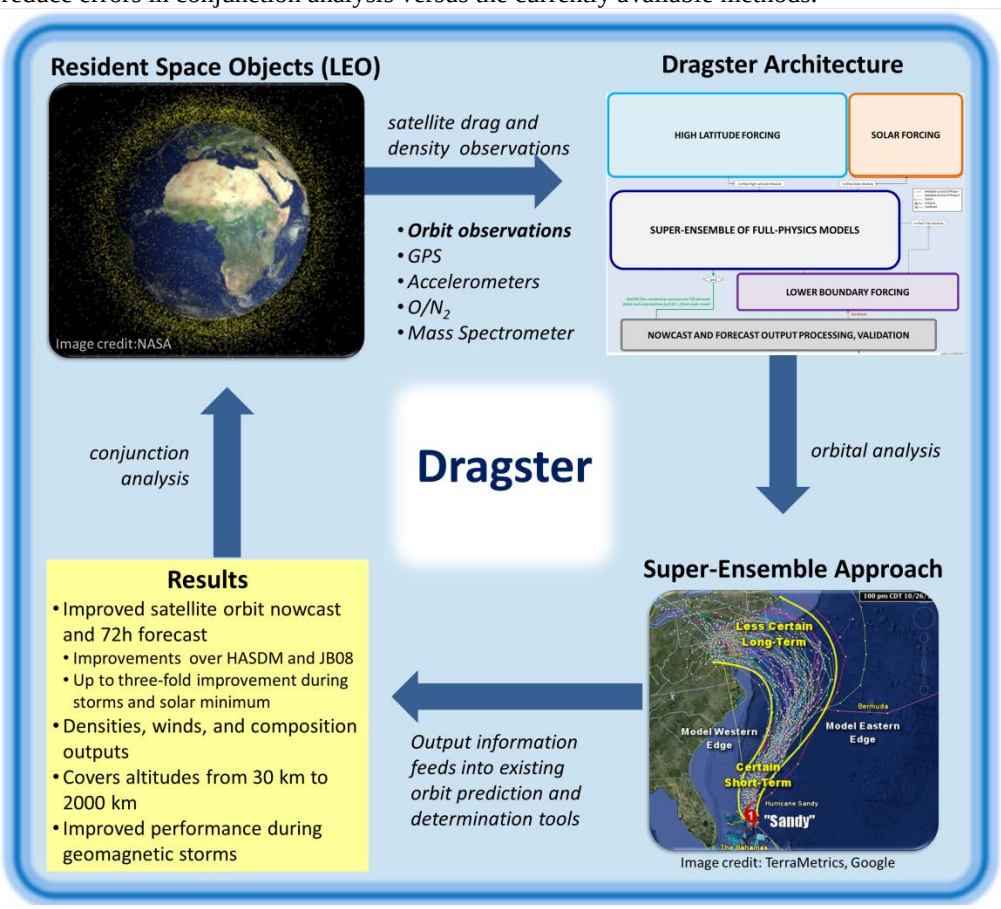


*Fig. 1: Dragster concept summary.*

In this paper we introduce the satellite drag problem and describe ongoing efforts to construct a new assimilative satellite drag model called Dragster. Dragster takes advantage of new assimilative techniques for space weather systems as well as an improved representation of atmospheric dynamics. We will review preliminary validation results of the Dragster model and describe some of these results in terms of orbital propagation errors.

## 3. THE SATELLITE DRAG PROBLEM

Satellite drag varies strongly as a function of the neutral thermospheric density and the satellite ballistic coefficient. Aerodynamic drag acceleration ($a_{drag}$) is expressed by the equation below in terms of atmospheric density ($\rho$), drag coefficient ($C_D$), cross-sectional area ($A$), spacecraft mass ($m$) and the spacecraft velocity relative to the atmosphere ($V_r$).

$$a_{drag} = \tfrac{1}{2}\rho \frac{C_D A}{m} V_r^{\,2} \tag{1}$$

The drag acceleration is the aerodynamic acceleration projected in the direction of satellite velocity. Many satellites also experience non-negligible lift forces which can cause long-term changes in the orbital inclination as well as aerodynamic torques which can alter the attitude state of the satellite.

The inverse ballistic coefficient is often used to describe the non-atmospheric contributions to satellite drag as shown below.

$$B = \frac{C_D A}{m} \tag{2}$$

In this paper, we will also use the term ballistic coefficient to refer to this term. Thermospheric mass density is the most variable of the parameters in Equation 1with mass densities ($\rho$) at a constant altitude changing by as much as 200-800% due to changes in geomagnetic activity levels (in other words, during solar storms) [1]. Here we have defined the variability as the total change of a parameter (in this case neutral atmospheric mass density, or simply atmospheric density) divided by the initial value of the parameter. In general, thermospheric density demonstrates variability with latitude, longitude and time due to variable internal forcings such as lowe-atmospheric dynamics and waves, and external forcings, by solar EUV flux changes and solar wind disturbances. The product of $C_D$ and $A$ is the second contribution to satellite drag variability with variations for elongated satellites flying above 180 km as large as approximately 100%.[2,3] Another 25%-50% change can be expected in the product of $C_D$ and $A$ below 180 km due to transition-flow effects [4,5]. Changes in atmospheric winds can lead to changes in $V_r$ as well and this can cause changes in satellite drag which are on the order of 3% 1-σ with maximum effects on the order of 13% during large geomagnetic storms [6].

## 4. OVERVIEW OF THE DRAGSTER MODEL

Dragster is designed to provide satellite-drag specification for the majority of resident space objects (see altitude distribution below) in the region where drag is the most relevant non-conservative orbital perturbation. This region is also populated with critical military, government, and commercial space assets. Dragster will specify real-time and forecast densities, compositions, and winds along satellite orbits to compute accurate drag estimates.

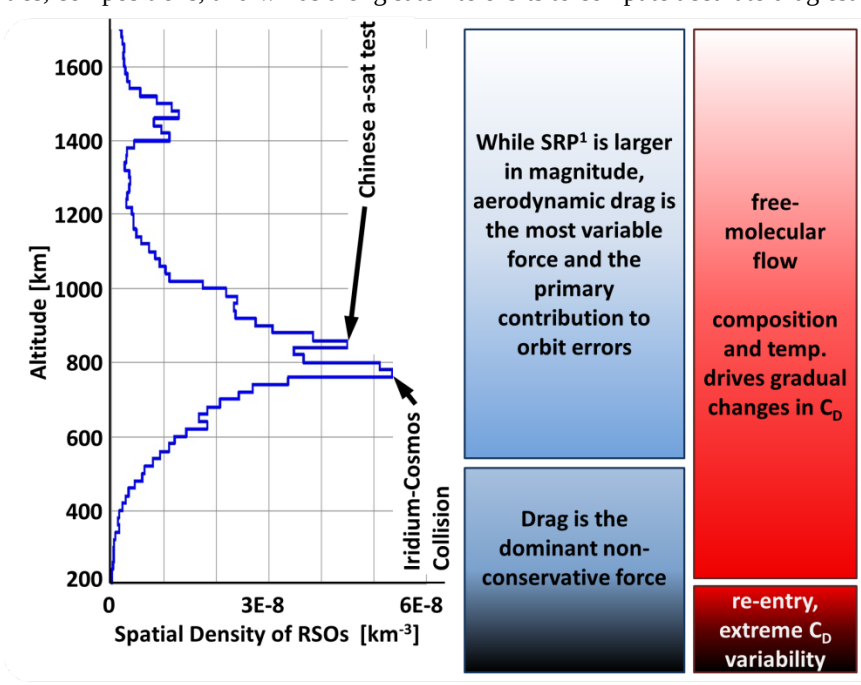


*Fig. 2. Altitude Regions of Relevance to Satellite Drag Specification. ([1]Solar Radiation Pressure)*

Requirements for the Dragster model nowcast and 3-day forecast are given in the table below. Note that the requirements and goals are based on performance as compared to the leading empirical drag model, Jacchia-Bowman 2008 (JB08), and the leading assimilative empirical model, High Accuracy Satellite Drag Model (HASDM) which is used operationally at the Air Force. In addition to these requirements, the Dragster software must also run within three hours of real time. This means that the nowcast (and the associated 3-day forecast) is no more than three hours latent from the time for which it was generated. In order to be used for drag specification, the model must also output self-consistent densities, winds, temperatures, and compositions along an arbitrary satellite orbit.

The JB08 and HASDM models represent the current state of the art for satellite drag prediction. The JB08 model is an empirical atmospheric density model used by the AF for satellite orbit prediction. The High Accuracy Satellite Drag Model (HASDM) dynamically calibrates a background density model such as JB08 by finding the least squares solution to the model temperature fields at both the "inflection altitude" (~120 km) and in the exosphere. Six hour orbit fit-spans from between 70-90 "calibration" satellites are used by HASDM to determine the spherical expansion of the atmospheric temperature fields. The solved spherical harmonic coefficients and their short-term trends can then be incorporated into an empirical model such as JB08 along with prediction indices to run a 3 day forecast of atmospheric density.

For all their capabilities, the uncertainties in JB08 and HASDM are still too large to satisfy the operational requirements of the Air Force. In fact, the Air Force Space Command (AFSPC) requirement is neutral density forecasts within 5% over a 72 hour period, something which the present state of the art (HASDM and JB08) does not provide.

**Table 1: Top Level Dragster Requirements.**

| | **Requirement** | **Goal** |
|---|---|---|
| **Nowcast** | Density errors lower than JB08 more than half the time. JB08: 13-18% at 200-800km | Density errors better than HASDM more than half the time. HASDM: 6-8% at 200-800km |
| **72h Forecast** | RMSE lower than JB08 in forecast mode | RMSE lower than HASDM in forecast mode |

The Dragster model is based on several empirical models as well as three well-validated Global Circulation Models: (a) the Thermosphere Ionosphere Electrodynamics Global Circulation Model (TIE-GCM), (b) the Thermosphere Ionosphere Mesosphere Electrodynamics Global Circulation Model (TIME-GCM) which includes coupling into the mesosphere, and (c) the Coupled Thermosphere Ionosphere Plasmasphere electrodynamics (CTIPe). For satellite drag applications, the global neutral density field is obtained from the thermospheric sections of these three codes. The neutral atmosphere codes solve the non-linear momentum, energy, and composition equations time-dependently over the globe, to provide neutral dynamics, temperature, and the distribution of neutral species. The three-dimensional distribution of neutral density is obtained from the temperature and composition, which together with the neutral winds provide the necessary parameters for satellite drag prediction. The self-consistent ionosphere is important and necessary to ensure the accurate conductivities, for characterizing high latitude Joule heating, for ion drag, and for realistic wind determination.

TIE-GCM, TIME-GCM, and CTIPe are used in an assimilative architecture within the Dragster model. Each model type is used to perform ensemble assimilation and hence the various models will sometimes be referred to as super-ensemble members. Dragster propagates the model ensemble members forward to predict the most probable trajectory of the thermospheric state and its uncertainty based on inter-model differences. It must be kept in mind that unlike tropospheric weather, the thermosphere is strongly driven by external inputs and depends less on the current and prior states. Therefore, future incorporation of state-of-the-art operational input forecasts will play an important role in reducing satellite drag errors.

## 5. DRAGSTER SOFTWARE DESCRIPTION

The Dragster software modules are outlined by thick boxes in Fig. 3. Three boxes represent model drivers: (a) the High-Latitude Forcing Subsystem (light blue); (b) Solar Forcing Subsystem (orange), and; (c) the Lower Boundary Forcing Subsystem (purple). These inputs are used to drive a series of full-physics models in the Super-Ensemble Subsystem (dark blue). The Super-Ensemble Subsystem generates model nowcasts and forecasts out to 72 hours

along with estimates of uncertainty. The output model fields are then processed by an Output Processing and Validation Subsystem (grey).

The High-Latitude Forcing Subsystem provides information on high latitude ionospheric convection patterns, coupling between the magnetosphere and ionosphere, and on Joule heating. The Solar Forcing Subsystem specifies UV/EUV fluxes impinging on the upper atmosphere. The Lower Boundary Forcing Subsystem specifies the impact of eddy diffusion and tides on the upper atmosphere. For each of the Forcing Subsystems, relevant data on current conditions can be obtained from a wide variety of measurement and model sources and can be configured by the user. In addition, in order to meet the requirement of 72-hour forecasting, the Forcing Subsystems all provide forecasts of the forcing parameters.

The Super-Ensemble Subsystem (dark blue box in the center of Fig. 3) consists of three full-physics models that are driven by the selected inputs described above. An ensemble of each model-type is run. The Dragster system uses a version of the Ensemble Kalman Filter (enKF) to provide nowcasts of various atmospheric and drag parameters although an Ensemble Optimal Interpolation (enOI) scheme is expected to be available in future versions. In the EnKF scheme, data is assimilated into every instantiation of each model type (green and blue boxes in the Super Ensemble Subsystem). The assimilation data is represented by the white boxes labeled "Assimilation Drag Data", and could include accelerometer data, and drag inferred from orbital observations.

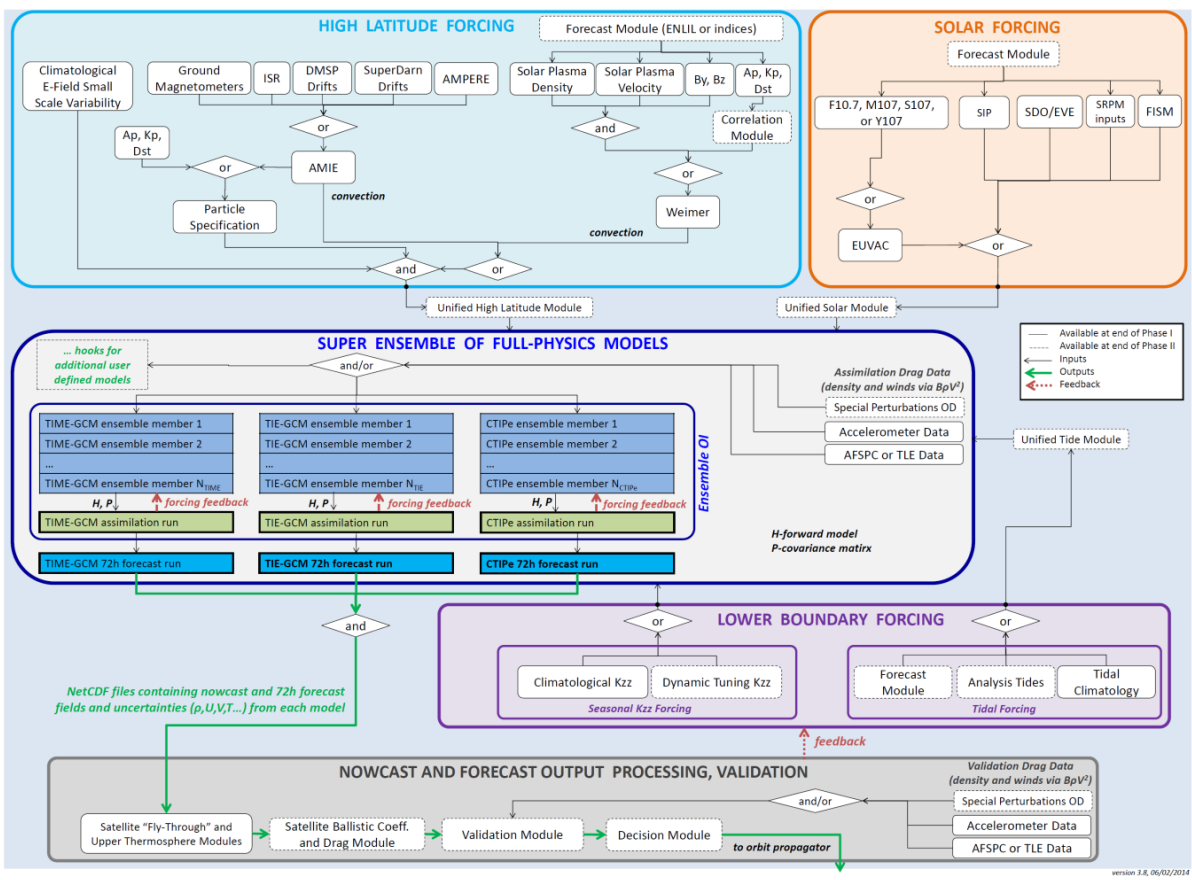


*Fig. 3. A conceptual flow-diagram indicating how the three GCM models are to be driven and how the various software modules interact.*

Fig. 4 shows the Dragster EnKF algorithm flow diagram. The algorithm begins in the upper left with the definition of the initial atmospheric state ($\mathbf{X_0}$) for every ensemble member. The states include a selectable span of model times to accommodate multi-bandwidth datasets. The software propagates all the atmospheric states to the current time and ingests new satellite drag data if it is available. At this point, the ensemble is used to compute the covariance matrices and the Kalman gain. Then, a solution $\mathbf{X_a}$ is obtained for each ensemble member and the average of these solutions ($\mathbf{x_a}$) is used to initiate a forecast of satellite drag parameters (i.e. densities) to be used for conjunction

analysis and orbit prediction. This part of the process is performed iteratively until a pre-specified convergence criterion is met. The iteration and wide time-range incorporated into each state cause this part of the algorithm to resemble a batch processor within an EnKF architecture. This approach along with the inclusion of atmospheric forcings in the state vector has been found to outperform other DA methods when assimilating data into strongly forced systems such as the Earth's upper atmosphere. Dragster then performs a re-sampling of the states based on the current state behavior taking into account the statistical distribution of the forcing parameters. At this point, the algorithm returns to the upper left hand of the flow-diagram and repeats.

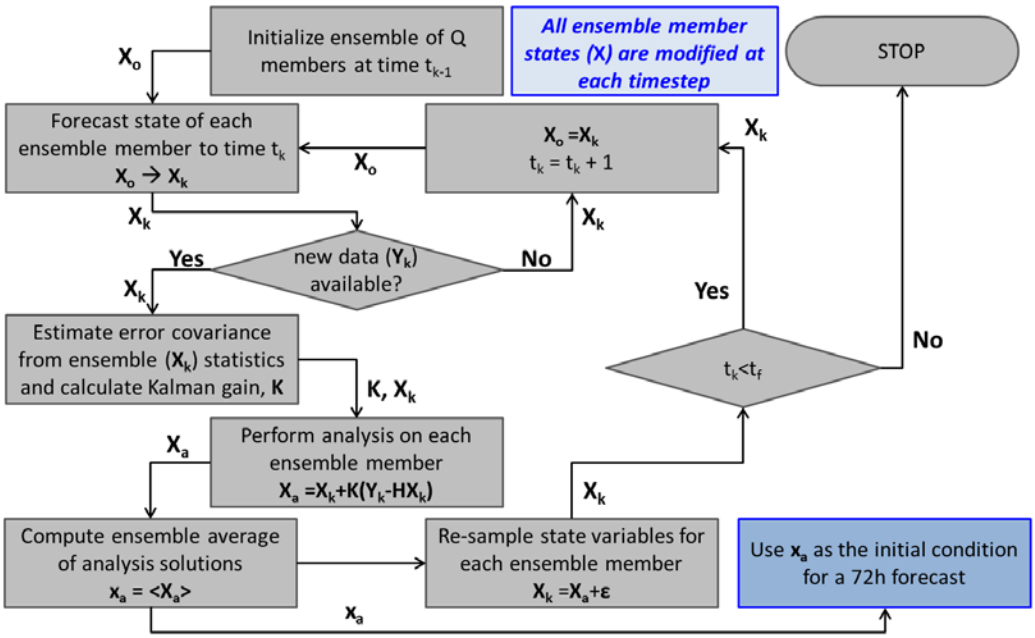


*Fig. 4: Ensemble Kalman Filter architecture in the Dragster software.*

The assimilated state $\mathbf{x_a}$ includes forcing parameters. An instructive test of forcing parameter assimilation is to assimilate synthetic data generated using one model, into an ensemble of that same model. Any resulting discrepancy is due to "process" noise associated with the data bandwidth limitations. In the test case presented below, TLE's were used as the input data. Fig. 5 shows the results of such a test using the Naval Research Laboratory Mass Spectrometer and Incoherent Scatter with Exosphere 2000 model (NRLMSISE-00, sometimes referred to MSIS) as the background. Here, forcing parameters include Ap (geomagnetic forcing) and F10.7 (solar radiation forcing). The figure shows four time series over the course of four months in 2015. The four time series include measured F10.7 flux (black), F10.7 flux estimated by Dragster (blue), the Ap planetary geomagnetic index (red), and the Ap estimated by Dragster (green). Both the F10.7 proxy and Ap index are plotted on the same y-axis scale. Normal day to day and seasonal variation in solar activity is represented in the plot. A geomagnetic storm in the middle of March is apparent as a sharp peak in the Ap index. The forcing parameters are recovered quite well in this test and the validation density residuals (density errors for satellites not assimilated into the model) were in the 1-2% range.

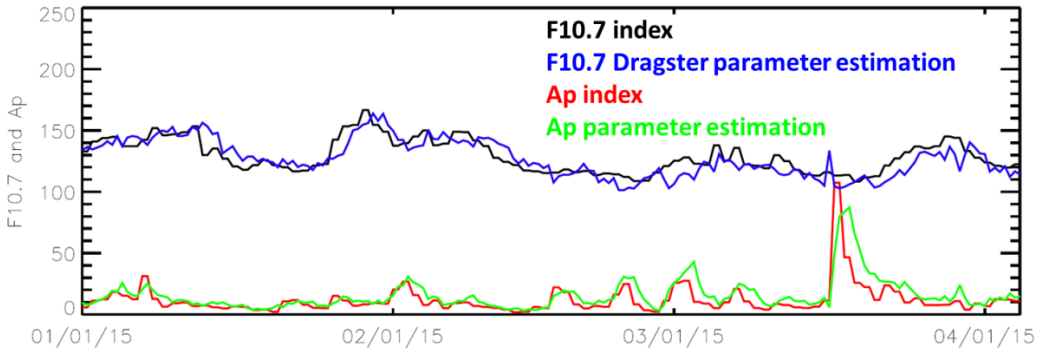


*Fig. 5: Forcing parameter estimation test using synthetic data and the NRLMSISE-00 model shows the ability to recover atmospheric forcing using imperfect satellite drag data.*

Every three hours, the assimilated states (which include the forcing parameters) will be used to initiate three 72 hour forecasts (one for each model type). Note that to the extent that forecast indices can be provided 7 days in advance, Dragster could also perform a 7-day forecast. The nowcast and forecast coming from each model-type is passed out of the Super Ensemble subsystem (green line in Fig. 4) as NetCDF files containing density, wind, composition, and temperature fields for each model at the nominal grid resolution. The NetCDFs are passed to an Output Processing and Validation Subsystem (grey box at bottom of Fig. 4).

In the Output Processing and Validation Subsystem, a satellite "Fly-Through" module computes the mass-density, neutral winds, number densities, and temperatures along any specified satellite orbit or series of orbits. These along-orbit parameters are passed to a Ballistic Coefficient and Drag Module, which uses them to compute a physics-based drag coefficient and an estimate of the satellite drag force along the orbit. In addition to implementing physics-based gas-surface interaction behavior into the ballistic coefficient prediction, Dragster software has the capability to include detailed aerodynamic models for all or some of the satellites. This allows assimilation of data from objects whose A/m ratios are not necessarily constant but are variable in a predictable way. This capability means Dragster can ingest more data than the current atmospheric-calibration tools. A panel model implements analytical free-molecular flow equations on an arbitrary array of flat-panels (one side exposed to the flow). Attitude is specified by defining the pointing mode for the satellite. For many objects, this specification is done heuristically wherein the satellite attitude is a well-defined function of the orbital position. The benefit of this approach is that it expands the database of beneficial assimilation objects but does not require additional auxiliary data (spacecraft pointing) to be ingested into the model. Fig. 6 shows examples of panel models used by Dragster including the SORCE, GRACE, and C/NOFS satellites. Panel models have also been generated for a number of other spacecraft used for validation and assimilation.

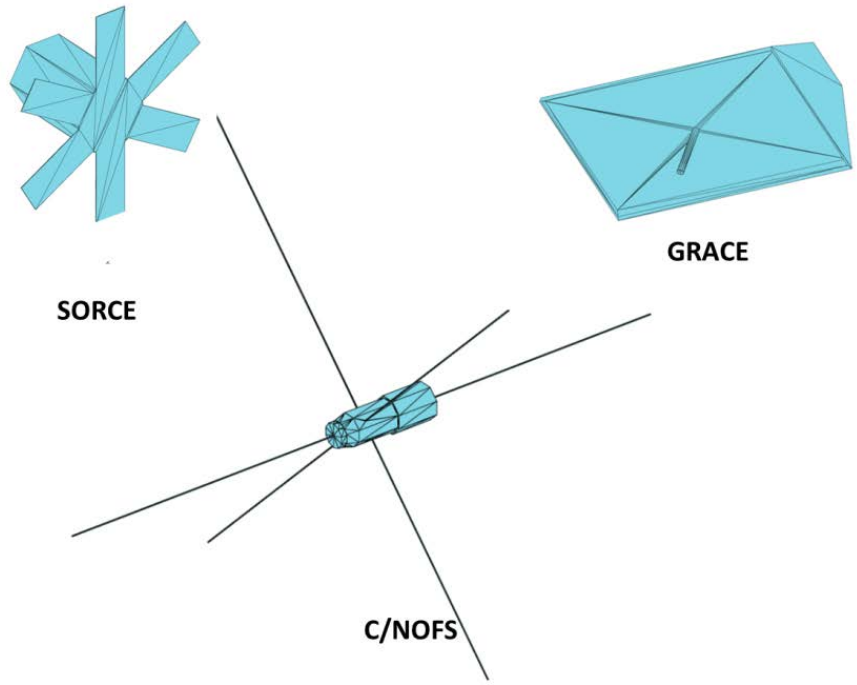


*Fig. 6: Examples of Dragster aerodynamic panel models.*

The Ballistic Module also computes a fitted-ballistic coefficient and examines its multi-year history for any object if a long enough dataset is available. In this way, a long-term average ballistic coefficient, and the best physics-based drag coefficient can be combined to provide a best estimate of satellite area-to-mass ratio to be used in the orbit propagation. The modeled drag force along the satellite orbit is passed to the Validation Module, which uses the information to compute the effective density or energy dissipation rates for a collection of validation objects that were not used in the assimilation. Energy dissipation rates and effective densities are defined in the next section. The validation data can include accelerometer or orbit-averaged drag measurements. The Validation Module compares the measured and modeled effective densities for each object and estimates a series of metrics for the nowcasts and forecasts.

Note that three validation methods are occurring at all times within the Dragster system. The first is an inherent validation, which occurs as a result of the assimilation in the Super Ensemble Subsystem. In this validation, assimilation data is compared with the assimilated model state (green box outputs) to compute drag residuals. The second type of validation is the Cross Validation occurring in the Output Processing Subsystem (grey box) for nowcast outputs. The third is the Forecast Validation occurring for the 72-hour forecasts. All three validation metrics are made available to the Decision Module which uses them to combine the assimilated model outputs (NetCDF files) into a single stream of densities, winds, compositions, temperatures, or drag predictions (as desired by the user). The operator chooses whether the Decision Module should apply outlier rejection, simple averaging, weighted-average based on the validation metrics for each model, or simply to choose one model for all times. The result is the best orbit-resolved drag nowcast and 72-h prediction updated every three hours, together with uncertainties in the predictions. This result can be passed to an orbit propagator of the user's choosing (external to Dragster).

## 6. TEST DATA

As mentioned in the previous section, the Dragster model can ingest both accelerometer as well as orbit-averaged drag data. Additional inputs such as composition measurements (from mass spectrometers and imagers) and atmospheric winds will be included as input options in the future. ASTRA has been testing the model architecture with satellite drag data using two-line-elements, daily-averaged densities, and accelerometer data as sources. Observation objects were selected according to a set of simple criteria. Selection criteria include a known shape which exhibits little variation in the observed ballistic coefficient, a stable fitted ballistic coefficient, or a ballistic coefficient of a known shape whose orientation with respect to the free-stream changes in a known way. These

criteria allow the ballistic coefficient to be estimated by both apriori means as well as by orbital observation. The current goal is to maintain a catalog of 50-100 assimilation/calibration objects and 10-15 validation objects. The validation objects are not used in assimilation but instead serve as independent evaluations of assimilation performance. The Dragster object list currently includes 75 assimilation/calibration objects and 14 validation objects which is within our goal. A wide range of inclinations and perigee heights allows Dragster to be sensitive to density changes at all latitudes and altitudes of interest. Fig. 7 illustrates a selection of some of the objects in the Dragster catalog. Although our current object-selection criteria have been adequate to demonstrate Dragster performance, we anticipate that performance will significantly improve when using the higher-quality special perturbations (SP) orbit fits. This is because the SP data generally has a higher cadence and smaller errors than the publically available data source currently used by Dragster.

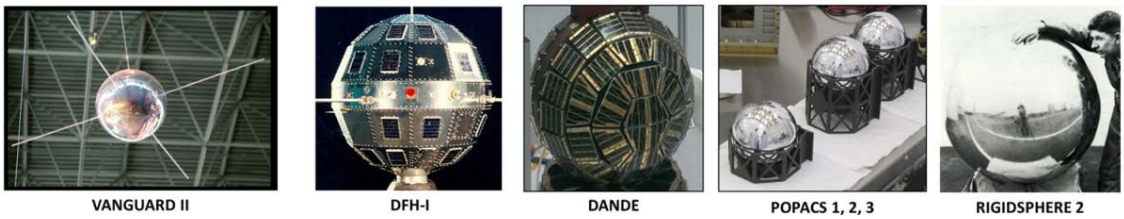


*Fig. 7. Examples of the test dataset for Dragster.*

Fig. 8 shows the locations of data from 75 satellites along with several validation satellites being assimilated into Dragster. The plot on the right shows the locations of assimilation (red) and validation (blue) orbits superimposed on a local-time/latitude map of atmospheric density at 400km altitude (greyscale). This coordinate system is used in Dragster (as it is in HASDM) because the structure of the upper atmosphere can be well-represented in a latitude local-time height coordinate system. Only the parts of the orbit most effected by satellite drag are shown (where each satellite experiences 80% of the drag withing the assimilation epoch). Validation orbits are shown in blue and correspond to data sources which are not assimilated and are only used to check (validate) the performance of Dragster. The plot on the left side of Fig. 8 shows the locations of the same assimilation (red) and validation (blue) orbits on a local-time/altitude reference frame. Note that shorter red and blue streaks correspond to more elliptical orbits which "dip" into the atmosphere in a more localized way. These objects are affected by smaller scale features which are not represented in the current operational drag models. Validation and Assimilation data in the tests presented here includes much of the atmosphere below 700 km. Dragster extrapolates results beyond 700 km if needed and ASTRA is currently working to including satellites in higher-altitude orbits (700km to 1000 km).

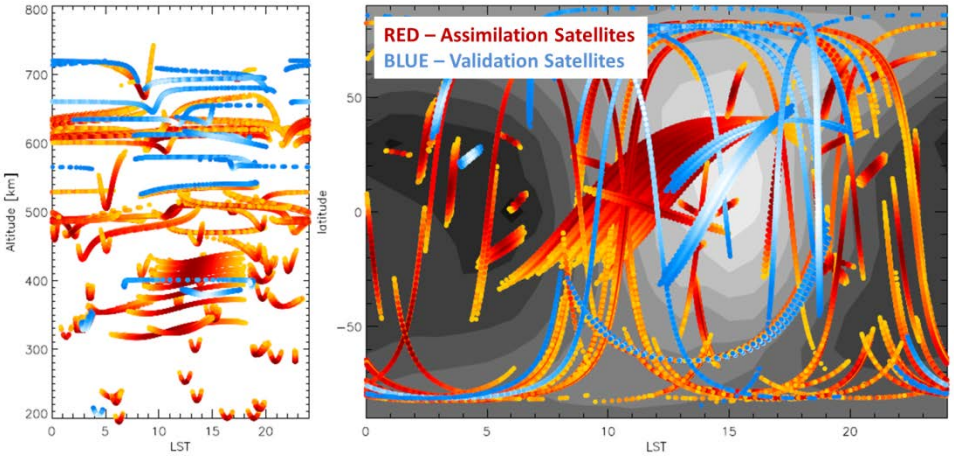


*Fig. 8: Local time, latitude, and altitude distribution of assimilation and validation satellites.*

In order to generate data for Dragster assimilation/calibration/validation objects, Dragster converts the orbital elements of the satellites in its dataset into energy dissipation rates (EDR) and effective atmospheric neutral densities. EDR's are the general drag assimilation metric for Dragster. This is because they can be easily extended to multiple satellite-drag data sources. This data is used as a stand-in for eventual high-task orbital tracking data processed using a special perturbations approach. The TLE dataset is not as accurate as the special perturbation approach and has a significantly lower bandwidth (2-4 day cadence). However it is freely available and has very

similar spatial sampling properties to operational datasets making it ideal for worst-case testing of our approach. The observed energy dissipation rate between times $t_i$ and $t_k$ is generated using the following relationship.

$$\dot{\varepsilon}_{\text{obs}}(t_{ik}) = \frac{\Delta n}{3 n_A \mu^{-2/3} \Delta t} \tag{3}$$

where $\mu$ is the Earth's gravitational parameter, $\Delta n$ is the change in the mean motion orbital parameter,

$$\Delta n = n(t_k) - n(t_i) \tag{4}$$

$n_A$ is the average mean mean-motion orbital parameter,

$$n_A = (n(t_i) + n(t_k))/2 \tag{5}$$

and $\Delta t$ is the length of time elapsed

$$\Delta t = t_k - t_i \tag{6}$$

The effective density ascribed to this observation is

$$\rho_{\text{obs}}(t_{ik}) = \frac{2 \cdot \dot{\varepsilon}_{\text{obs}}(t_{ik}) \cdot \Delta t}{B \cdot \int_{t_i}^{t_k} V_{\text{sc}}^{\ 3} F dt} \tag{7}$$

where $V_{sc}$ is the spacecraft velocity and $F$ is the wind factor.

An additional source of validation data used were densities derived along the orbit of the GRACE satellite from on-board accelerometer measurements. The two identical GRACE-A and GRACE-B satellites were launched into an approximately 500 km near-circular orbit with an inclination of 89.5° on March 2002. The two GRACE satellites fly in a leader-follower formation and are nominally separated by 200 km. Note that in the analysis of GRACE densities, only the GRACE-A satellite is used. The GRACE accelerometer-derived densities were calibrated to TLE-derived densities for the GRACE satellite. To do this, an accelerometer x-axis bias factor was computed daily during each contiguous timespan of data (days of year 7-133, 173-280, and 342-365). Next a linear fit was performed to the daily bias factors in each contiguous data segment. These linear fits were used to calibrate the accelerometer data. Note that this GRACE dataset provides 256 days of data in 2015 due to spacecraft maneuvers during two times of the year. Specifically, there are two swaps of the A and B GRACE satellites between the forward/rear flying position, which removes a significant amount of useable data for the year. The first swap is in May-June, while the second one is around November.

Furthermore, neutral densities measured by the CHAMP satellite accelerometer are used to evaluate the efficiency with which physics-based background models reproduce space weather related enhancements in neutral density and satellite drag during geomagnetic storms. Version 2.3 of the CHAMP density database [7, http://impact.lanl.gov/data/ver2.3/champ/DataReleaseReport.pdf] was used. The CHAMP satellite was launched on July 2000 into a 450 km orbit, with an inclination of 87.3°. It reentered in September 2010.

## 7. PRELIMINARY VALIDATION RESULTS

For the preliminary evaluation, drag observations from the orbit data of 75 satellites was assimilated into Dragster using NRLMSISE-00 as the background model. The assimilation spans from January 2015 through December 2015. A 36 hour assimilation window was used with effective-densities spanning the 1.5 day time period advanced forward in time in 0.5 day steps. Dragster solar and geomagnetic forcing parameters as well as density corrections were being estimated using a 90-member ensemble. The spatial resolution for the density corrections was a 15°x15° latitude-longitude grid. Fig. 9 below shows the results of the densities from Dragster (gold), HASDM (green), MSIS (red), and JB08 (blue) models for the duration of 2015 compared with TLE-derived densities for the GRACE satellite (~400km altitude). Note that the assimilative Dragster results match very well with the densities experienced by this validation satellite (GRACE was not assimilated into Dragster nor was it assimilated into HASDM). Reproducing the variability seen below depends on accurately representing the seasonal variability in the atmosphere, local-time and latitude structure, response to solar and geomagnetic activity, and implementing an adequate representation of the satellite ballistic coefficients. It is important to note that while HASDM appears to

have the largest error, most of this offset is due to a bias between the model and our dataset. A more subtle look at validation errors will follow later in this section.

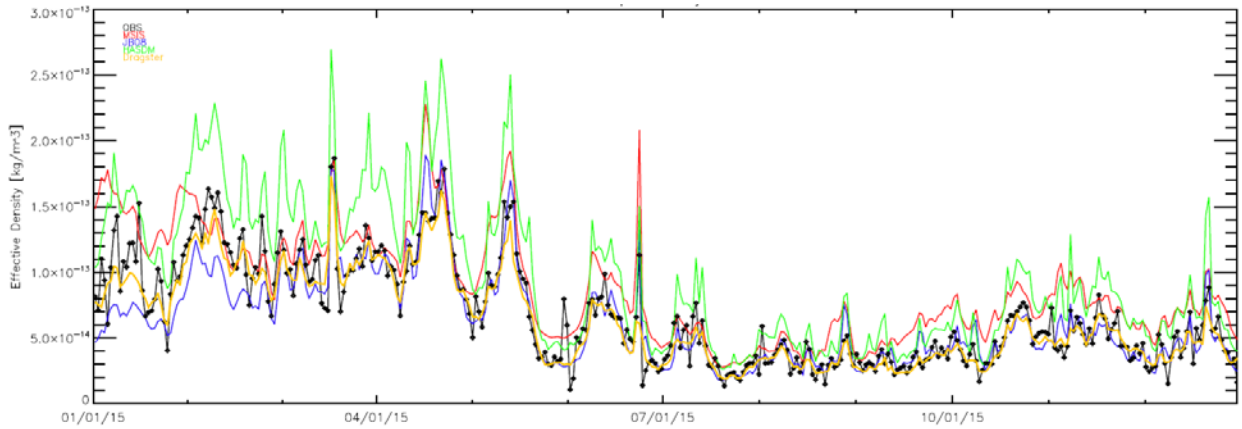


*Fig. 9: One-year time series of observed and modeled densities using the source satellite*

Fig. 10 illustrates the modeling results over four shorter timespans (20 to 50 minutes) throughout the evaluation year. The black line in the figure represents GRACE accelerometer measurements of atmospheric density, the other solid lines represent the assimilative models (HASDM in magenta and Dragster in blue) while the dotted lines represent the empirical models. Arrows in each panel indicate spatial structures modeled by Dragster and detected by the GRACE accelerometers which are not resolved by any of the other models.

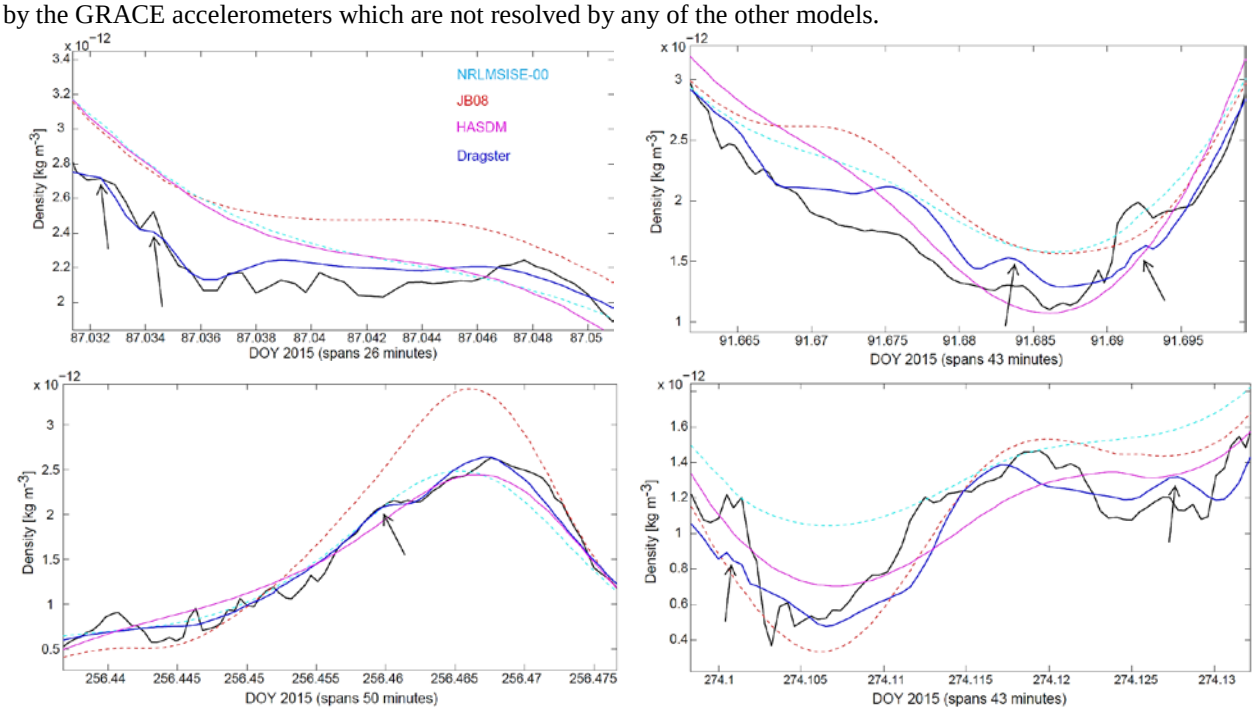


*Fig. 10: Data-model comparison showing small scale neutral density features emergent in the Dragster model.*

Even though these smaller-scale features are sometimes offset in magnitude from the GRACE observations, this is an issue which can be addressed by including a higher-cadence dataset in Dragster. This result confirms that Dragster can take advantage of localization to produce a more complete picture of the satellite drag environment.

Fig. 11 illustrates further analysis of model errors using the full validation dataset of 14 satellites. Standard deviation errors for each of validation satellites were computed throughout the 2015 evaluation period. The standard deviations for each validation satellite are divided by the standard deviation obtained using the JB08 model for that same satellite and plotted as a function of the satellite perigee altitude. In other words, if the relative standard deviation is unity (indicated by the horizontal dotted line) then the standard deviation for that model-satellite pair is equivalent to that of the JB08 atmospheric model. Values above the dotted line indicate model performance which

is worse than JB08 and values below the dotted line indicate performance which is better. The red triangles correspond to the background model used in this evaluation (NRLMSISE-00). The cyan diamonds with inset stars indicate HASDM errors (HASDM data was only available for four of the validation objects). The green diamonds indicate Dragster performance. Note that absolute JB08 errors are approximately 7% near 200km and increase to 18% near 700km altitudes. Note also that Dragster reduces the background model error for each object except for the satellite near 200km. Fig. 10 verifies that Dragster errors are lower than JB08 and are either better than or equivalent to HASDM satisfying the requirements set out in Table 1. Table 2 shows performance metrics for the validation objects for which HASDM densities were available. The validation metrics include standard deviation, bias, and prediction efficiency as defined by Shim et al. [8]. The values in the table demonstrate that Dragster outperforms the other three models in almost every category when TLE validation data is used for validation.

It is also instructive to validate the models against non-TLE data. To this end, we performed a spectral analysis of the density errors along the orbit of the GRACE satellite over the course of 2015 for each of the models. The GRACE accelerometer-derived densities were used as truth in the error computation. A Fast Fourier Transform (FFT) was performed on the dataset to compute the noise power spectral density (PSD) for each model. Next the noise PSD was integrated from a low-pass cutoff out to 180 days to demonstrate how the elimination of high-frequency noise affects the overall errors for each model. Fig. 12 shows the results of the FFT (left panel) and the integrated or total noise (right panel) on a logarithmic scale as a function of period. Vertical dotted lines indicate time scales of interest from 1-orbit to 1 month. The PSD plot shows that HASDM (red solid line) has the best performance (lowest noise levels) in the first half of the spectral region overlapped by the bandwidth of its operational input data (indicated by a red arrow in the figure). A blue arrow indicates the bandwidth of the TLE dataset assimilated by Dragster (blue solid line) and we observe that Dragster has superior performance within that bandwidth. We also see that in the 1-12 hour range, where neither model's input data has sufficient spectral content, the error of both HASDM and Dragster is similar to the performance of their background models (JB08 and MSIS respectively). In other words, there is no improvement in either Dragster or HASDM over their respective background models in this part of the spectrum. We expect further improvements in Dragster at these timescales when using first-principles background models such as TIE-GCM due to their better representation of smaller scale features. Below the time-scales of 1 hour, the performance for all models is equivalent although this performance is also expected to improve when using a first-principles background model. The integrated noise figures in the right hand panel of Fig. 12 show that as the low-pass filter cutoff is increases, the error for each model falls.

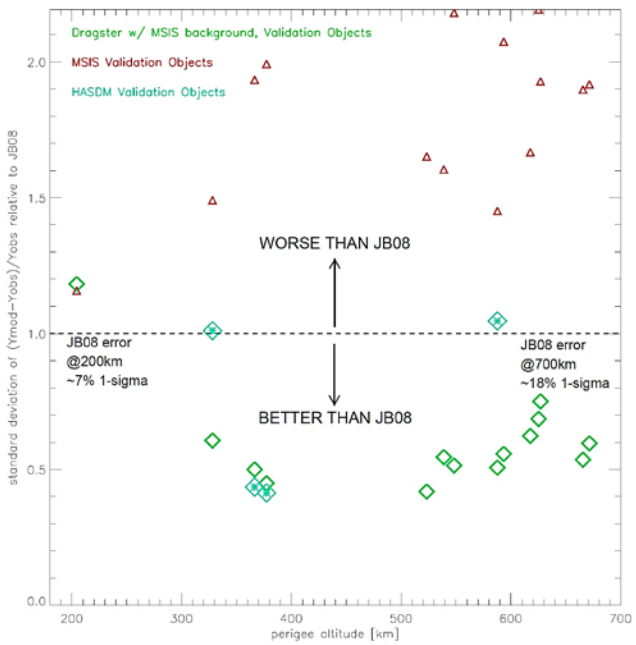


*Fig. 11: Standard deviation errors for all validation objects relative to JB08 standard deviations. Values above the dotted line indicate performance worse than JB08 while values below the dotted line indicate performance better than JB08.*

*Table 2: 2015 validation metrics for select satellites.*

| Satellite *NORAD ID Name (Altitude)* | Model[2] | Standard Deviation | Bias | Prediction Efficiency |
|---|---|---|---|---|
| #27651 SORCE (591 km) | M | 28% | 32% | 0.27 |
| | J | 20% | -7% | 0.53 |
| | H | 25% | 41% | 0.06 |
| | D | 15% | -7% | 0.68 |
| #40314 Spinsat (390 km) | M | 18% | 15% | 0.30 |
| | J | 11% | -12% | 0.39 |
| | H | 11% | 17% | 0.33 |
| | D | 8% | -11% | 0.46 |
| #39267 DANDE (338 km) | M | 24% | 38% | 0.31 |
| | J | 14% | 10% | 0.72 |
| | H | 17% | 42% | 0.10 |
| | D | 10% | 2% | 0.82 |
| #27391 GRACE-A (393 km) | M | 19% | 31% | -0.08 |
| | J | 11% | -0% | 0.63 |
| | H | 9% | 33% | -0.15 |
| | D | 7% | 0% | 0.76 |

[2] M-MSIS J-JB08 H-HASDM D-Dragster

The integrated Dragster performance is best above the 1-3 day mark where the bandwidth of its TLE dataset begins. In this context, the results obtained with TLE-based validation data are limited to the right hand side of Fig. 12 due to the bandwidth of those measurements. Again, we expect that performance enhancement to extend to higher frequencies (periods lower than 1-3 days) when we transition Dragster from TLE data to the SP input data.

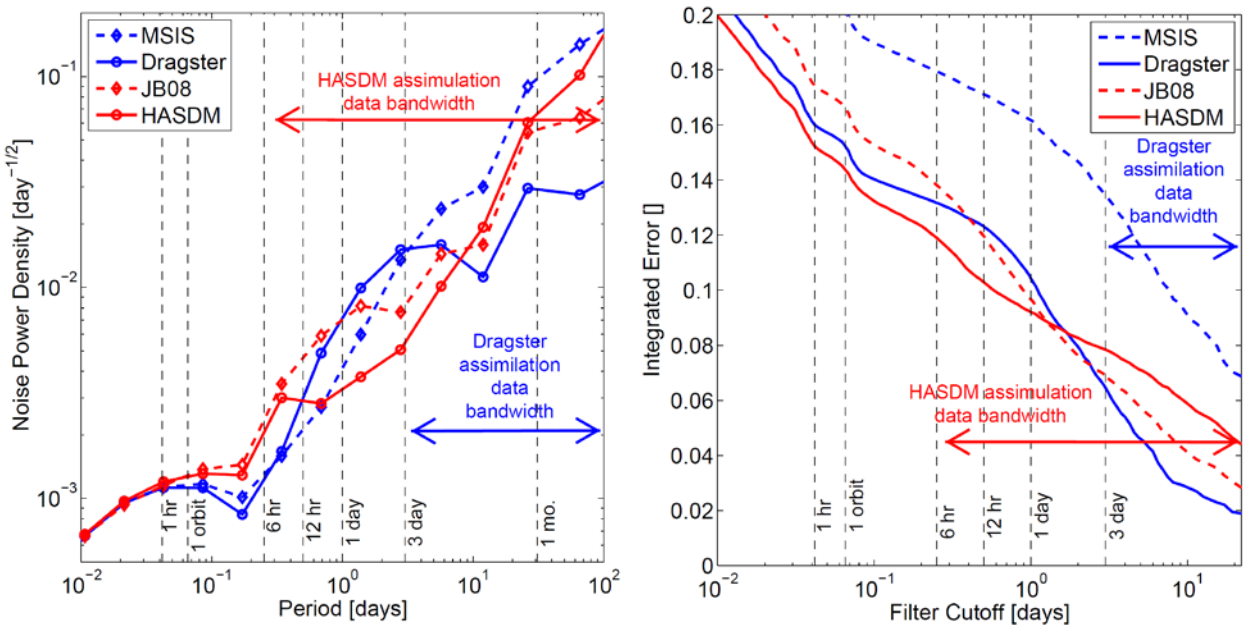


*Fig. 12: GRACE accelerometer data used to compute the spectral noise density (left) of various atmospheric models. The integrated error is represented as a function of a low-pass filter cutoff (right).*

## 8. VALIDATION OF ENHANCED GEOMAGNETIC STORM REPRESENTATION USING FIRST-PRINCIPLES MODELS

Geomagnetic storms present times of large atmospheric model error and therefore, large satellite drag and orbit prediction uncertainty. In fact, a large geomagnetic storm in March of 1991 led to severe orbit prediction errors and caused JSpOC to "lose" track of a couple hundred objects in its catalog. This storm was a major motivation behind work to improve atmospheric models and to transition HASDM into operational use at the DoD. Many geomagnetic storms since that time continue to motivate improvements in the representation of the atmospheric response for the purposes of satellite drag and orbit prediction. One such improvement has been shown to successfully reproduce the atmospheric response during storms by assimilatively specifying the geomagnetic energy input into the atmosphere. This assimilative technique is called AMIE, is integrated into Dragster to drive the TIME-GCM background model, and is run at ASTRA in realtime. Fig. 13 shows modeled and measured densities along the CHAMP satellite track during the 8/24/2005 geomagnetic storm. Each panel shows a comparison between measured (blue) and modeled (red) densities along the satellite track. The wavy lines show diurnal variation of atmospheric density in each orbit. Low densities at the beginning of the time period are characteristic of geomagnetically quiet times while the factor of 2-3 increased densities later in the time period are caused by the geomagnetic storm. Note that this will correspond to a factor of 2-3 increase in satellite drag and contribute to significant changes in the orbit. NRLMSISE-00 and JB08 are both empirical models that do not assimilate any data. JB08 does a poor job due to the Dst input index not capturing the energy input of this storm event and also due to the low spatial resolution of this model. MSIS does show a slight increased density during the storm but still missed the location of the high latitude density peaks. TIME-GCM is a physics based model and it clearly shows storm-enhanced densities, though it overestimates them significantly due to an overestimate in storm energy by the Weimer high latitude convection model. The best match to the data is provided by the Dragster model with AMIE assimilative high-latitude specification (bottom right). This shows that the assimilative runs vastly improve storm response modeling and the associated satellite drag specification.

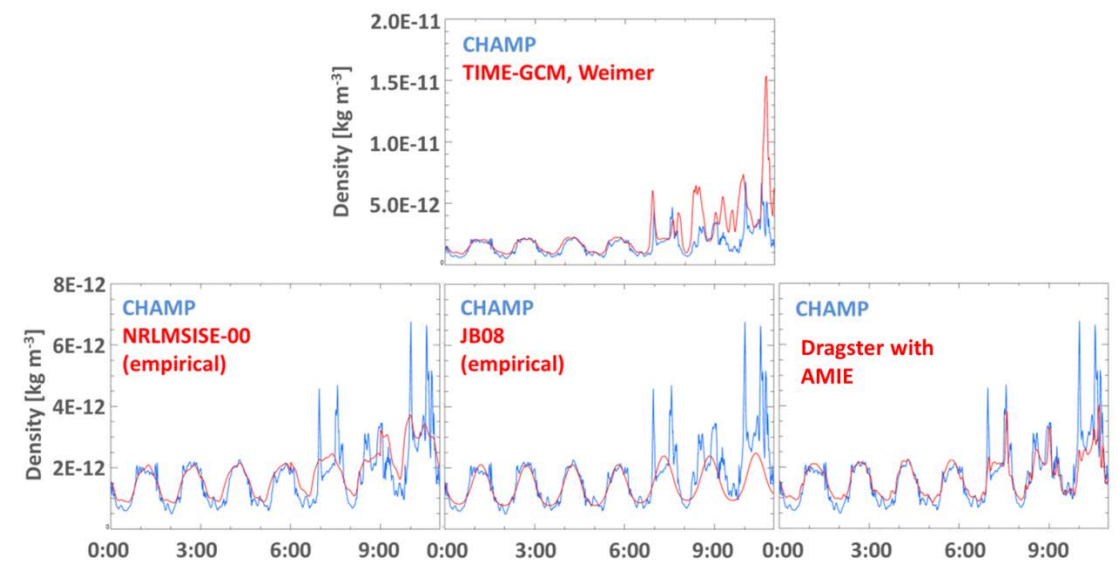


*Fig. 13. Time-series of model and measured densities along the CHAMP satellite track.*

## 9. MODELING RESULTS IN TERMS OF SATELLITE ORBIT ERRORS

We will now use modeled and measured (GRACE) densities to evaluate the drag force modeling on the GRACE satellite in an approximately 400 km circular orbit. The equations of motion for both the "truth" or GRACE-density case and the atmospheric-model cases were integrated using a Runge-Kutta 4-5 variable stepsize integrator. The area-to-mass ratio of the representative satellite was taken to be 0.0027 $m^2$/kg and the drag coefficient was

arbitrarily fixed at 3.2. The assumed ballistic coefficient is therefore 0.0088 $m^2$/kg and will be referred to as $B^*$. The drag coefficient is really not fixed along the orbit however it was desired in this case to separate the drag coefficient errors from those caused only by model densities. To further achieve this aim, a "fitted ballistic coefficient" ($B_{\text{fit}}$) was computed during each propagation timespan. The ballistic fitted coefficient for an epoch beginning with time $t_i$ and ending at $t_k$ was computed as follows:

$$B_{\text{fit}}(t_{ik}) = B^* \frac{\int_{t_i}^{t_k} \rho_{\text{accel}} V_{\text{sc}}^{\ 3} F dt}{\int_{t_i}^{t_k} \rho_{\text{model}} V_{\text{sc}}^{\ 3} F dt} \tag{8}$$

At each orbit propagation epoch, the ballistic coefficient computed in the previous epoch is used. In this way, the process of forecasting an orbit is emulated. To some extent, this removes some of the low-frequency noise and bias seen for certain models in Fig. 9.

Propagation epoch spans of 12hr, 24h, 72hr (3 days), and 168hr (7 days) were used. Only gravitational forces (including J2) and satellite drag were considered in the equations of motion. Three atmospheric models will be compared with the GRACE drag measurements:

- NRLMSIS-00 (MSIS) empirical model (no assimilation)
- Dragster with an MSIS model background assimilating TLE-derived drag products with a 1-σ error of approximately 5% and cadence of 2-4 day. The number of assimilation objects is 75. GRACE data is not assimilated into Dragster.
- HASDM with Jacchia-like model background assimilating SP orbit products from AF high-task tracking data having a 1-σ error of approximately 1-2% and cadence between 6 hours and 3 days. The number of assimilation objects is 80-90. GRACE data is not assimilated into HASDM.

Fig. 14 shows a time series of model errors in the early part of 2015 using a 72 hr timespan for orbit propagation. Note that the use of both HASDM and Dragster (assimilative models) result in errors smaller than the orbit propagation performed using the empirical (non-assimilative) MSIS model. A good example of the differences in performance resulting from the use of various atmospheric models is seen just before Day of Year 80 when a geomagnetic storm associated with Ap values in excess of 100 caused sharp increases in the atmospheric density and in satellite drag. During the storm, 72 hour in track errors exceed 20km when using the MSIS model. However, the in-track errors when using Dragster during this time are 10km. The best performance in this case is achieved by HASDM with approximately 7km in-track errors incurred. It is important to note that the HASDM model in this test used SP orbit solutions which are of much higher cadence and have lower errors than the TLE data ingested into Dragster. We expect Dragster errors to decrease significantly when using such a dataset.

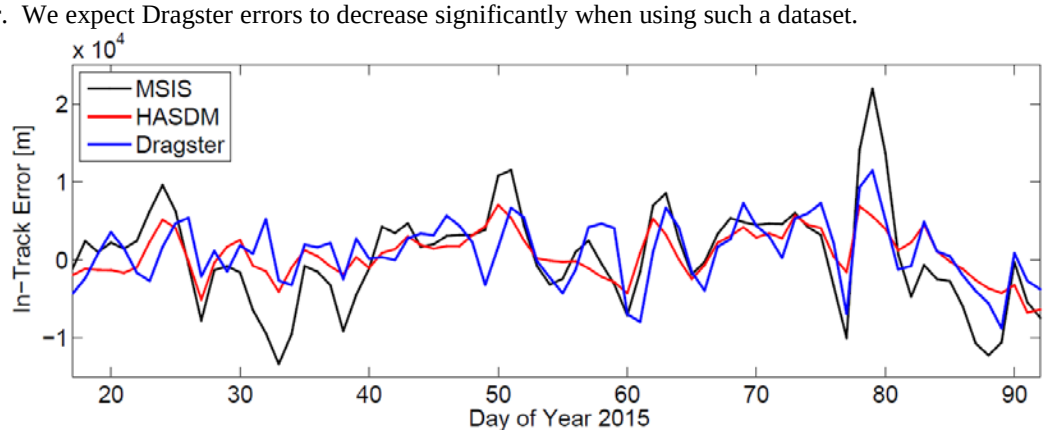


*Fig. 14: Time series of 72-hour in-track errors for the GRACE satellite near 400 km altitude. The larger errors just before Day of Year 80 occur during a strong geomagnetic storm.*

The in-track orbit errors from all orbit simulations are summarized in Fig. 15. The figure is composed of four panels, each corresponding to a different orbit propagation timespan (from 12hr in panel (a) to 7 days in panel (d)).

Each panel contains three box plots, one for each atmospheric model used in the orbit propagation. Box plot whiskers indicate the standard deviation (1-σ) around the mean. The red lines indicate the median of the error distribution while the red crosses are the mean of each error distribution. The extent of each blue box indicates the span of errors between the $25^{th}$ and $75^{th}$ percentiles of the distribution. Note that the x-axis in each panel (a-d) has a different scale. As is expected the orbit errors grow with increasing propagation time. The 1- σ errors are indicated in each panel and are approximately 300m for the 12 hour case and 20,000m – 40,000m for the 7-day case.

The relative advantage afforded by using assimilative atmospheric models increases with the integration timespan. This can be partly explained by the noise PSD profiles in the left panel of Fig. 12. The atmospheric model noise PSD indicates that orbit propagation with the Dragster model should have good performance in the region around 3 days (72 hrs) or more. This spectral region corresponds with panels (c) and (d) in Fig. 15 which confirm that the use of Dragster results in significantly reduced in-track errors over the empirical model (MSIS). The standard deviation for the in-track error distribution from a 7-day propagation using Dragster is less than half that when using the empirical model and approximately equivalent to the propagation using HASDM. It is also important to note that the previous-epoch fitted ballistic coefficient computation removes significant amounts of the bias at the periods above the propagation timespan. The fitted-ballistic coefficient procedure therefore approximates a high-pass filter allowing signal through at periods below the propagation time span. Because we see that the atmospheric model noise levels drop quickly towards lower periods (left side of the PSD in Fig. 12), applying a fitted ballistic coefficient to orbit propagation with short integration timespans should make the choice of model less important to the final outcome. Panels (a) and (b) of Fig. 15 indicate that this is indeed the case and that when propagating an orbit over 12 hr and 24 hr timespans respectively, the differences due to the various atmospheric models are much less pronounced.

A consistent feature of all in-track error distributions in Fig. 15 is a slight positive offset of their mean and median values from zero and is still under investigation.

Fig. 15 indicates that the orbit propagation performance (in-track errors) for Dragster and HASDM is approximately equivalent with HASDM resulting I slightly smaller in-track errors. Recall again that Dragster is driven only by TLE's in this test while HASDM has high cadence observations of satellite orbits. The number of assimilation/calibration objects ingested into both Dragster and HASDM is approximately equivalent but the HASDM operational dataset is much more accurate. We expect that future tests using SP orbit data for all Dragster assimilation objects would result in better performance relative to HASDM. Note also that the Dragster and HASDM standard deviations shown in Table 2 for the GRACE validation satellite were also quite similar (7% vs. 9%) so that similar orbit-propagation statistics are to be expected.

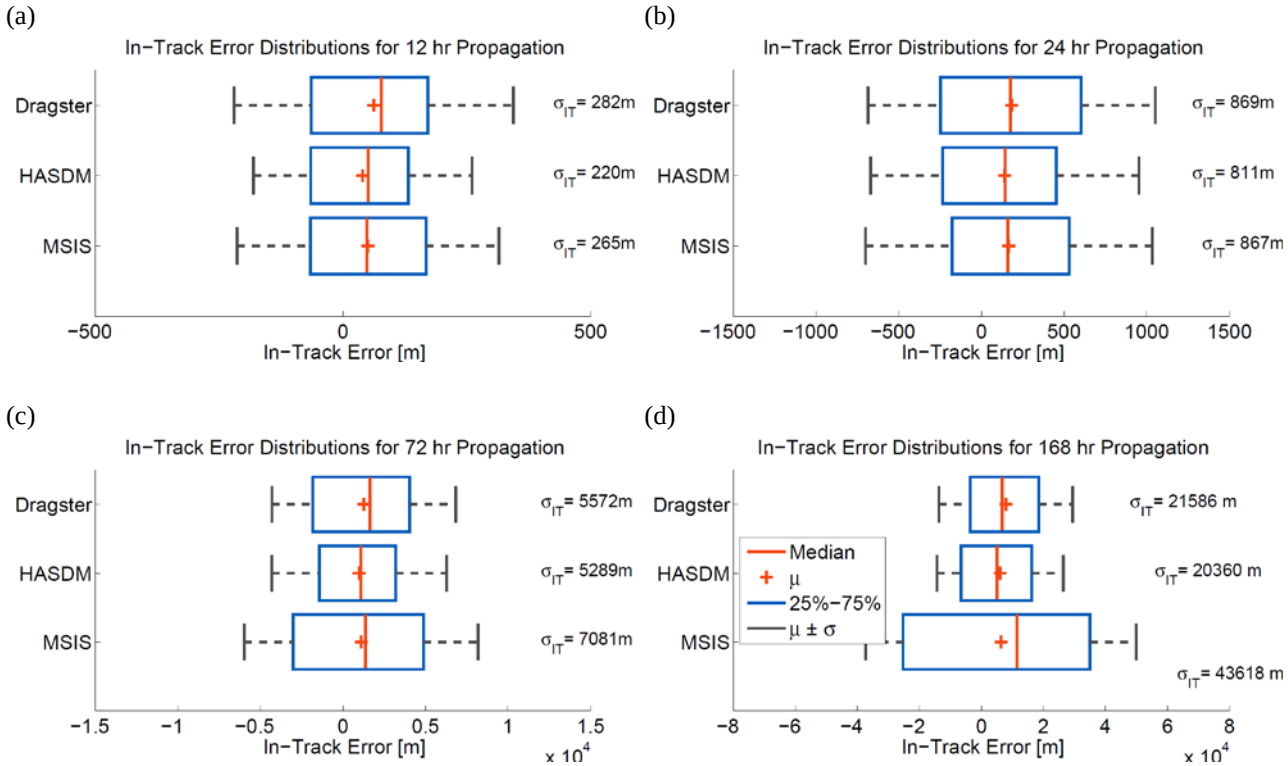


*Fig. 15: GRACE satellite orbit propagation statistics for in-track errors using atmospheric densities from three models compared with a propagation using densities measured by the GRACE accelerometers. Each box and whisker corresponds to either (1) Dragster assimilating TLE-based data from 75 satellites, (2) HASDM assimilating SP orbits from high task tracking of 80-90 satellites, or (3) empirical MSIS model w/o assimilation.*

## 10. CONCLUSIONS

A new state-of-the-art assimilative model of the atmosphere called Dragster is being developed at ASTRA in conjunction with its government and academic partners to improve satellite drag specification and forecast. The model incorporates many of the lessons learned from recent research in atmospheric dynamics and assimilation. In particular, the model development takes advantage of the AFOSR-supported Multi-University Research Initiative "Neutral Atmosphere Density Interdisciplinary Research" (NADIR) program. NADIR has laid the groundwork for the development of a first-principles assimilative operational model by deepening our understanding of the basic physical processes that drive the density and winds in the upper atmosphere.

The purpose of the Dragster development is to improve over operational drag-specification below 2000km altitudes in real-time and perform three-day or greater satellite drag forecasts. This altitude range has the advantage of capturing the majority of resident space objects that are affected by changes in the upper atmosphere. The Dragster project's success is evaluated by comparing its performance to empirical atmospheric models as well as the HASDM assimilative model. As we have shown in this paper, Dragster density nowcast performance is already better than that of empirical models even though tests were only run with empirical model background. Atmospheric density specification is equivalent to or better than HASDM according to TLE validation analysis. However we point out that these performance gains are limited by the bandwidth of the TLE test dataset. An analysis of orbit propagation performance for the GRACE satellite indicates that in-track orbit errors are equivalent to HASDM near 400km altitudes and improve over the use of NRLMSIS-00 for 3-day and 7-day orbit propagation timespans.

Future Dragster test and evaluation efforts will focus on testing with non-TLE (lower noise) assimilation data and including the first-principles models in the EnKF.

## 11. ACKNOWLEDGMENETS

This work was supported by Air Force contract FA9453-12-M-0091 (AFOSR). We thank the sponsor for their support.

## 12. REFERENCES

[1] Bruinsma, S. L., and J. M. Forbes (2007), Storm-Time Equatorial Density Enhancements Observed by CHAMP and GRACE, J. Spacecraft and Rockets, Vol. 44, No. 6, doi: 10.2514/1.28134.

[2] Doornbos E. (2011). Thermospheric Density and Wind Determination from Satellite Dynamics. PhD thesis, Delft University of Technology.

[3] Pilinski, M. D. and B. Argrow (2013a), Aerodynamic analysis based on CHAMP satellite lift-to-drag measurements, J. Spacecraft and Rockets, doi: 10.2514/1.A32394.

[4] Bowman B. R. and S. Hrncir (2007). Drag Coefficient Variability at 100-300 km from the Orbit Decay Analyses of Rocket Bodies. In AAS/AIAA Astrodynamics Specialist Conference, number AAS 07-262. AAS/AIAA.

[5] Pilinski M. D., B. M. Argrow, S. E. Palo, B. R. Bowman (2013b), Semi-Empirical Satellite Accommodation Model for Spherical and Randomly Tumbling Objects, Journal of Spacecraft and Rockets, Vol. 50, pp. 556-571, doi: 10.2514/1.A32348 .

[6] Crowley, G., Pilinski, M., and Azeem, I. (2012), Tutorial: The Neutral Atmosphere and the Satellite Drag Environment, AAS 12-035, 145-161.

[7] Sutton, E. K., R. S. Nerem, and J. M. Forbes (2007), Density and winds in the thermosphere deduced from accelerometer data, J. Spacecraft and Rockets, 44(6), 1210, doi:10.2514/1.28641.

[8] Shim, J-S, M. Kuznetsova, L. Rastaetter, M. Hesse, D. Bilitza, M. Burala, M. Codrescu, B. Emery, B. Foster, T. Fuller-Rowell, J. Huba, A. J. Mannucci, X. Pi, A. Ridley, Ludger Scherliess, Robert W. Schunk, P. Stephens, D. C. Thompson, Lie Zhu, D. Anderson, J. L. Chau, Jan J. Sojka, and B. Rideout (2011), CEDAR Electrodynamics Thermosphere Ionosphere (ETI) Challenge for Systematic Assessment of Ionosphere/Thermosphere Models 1: NmF2, hmF2, and Vertical Drift Using Ground Based Observations, Space Weather Journal, Vol. 9, S12003, doi:10.1029/2011SW000727.